Journal of Photochemistry and Photobiology A: Chemistry 346 (2017) 265–272

Contents lists available at ScienceDirect

Journal of Photochemistry and Photobiology A: Chemistry

journal homepage: www.elsevier.com/locate/jphotochem

Two new colorimetric and ratiometric fluorescent probes based on diketopyrrolopyrrole (DPP) for detecting and imaging of mitochondrial SO_2 derivatives in cancer cells

Jian Wang[a], Yandi Hang[a], Haoqi Tan[b], Tao Jiang[a], Xue Qu[b], Jianli Hua[a,*]

[a] Key Laboratory for Advanced Materials & Institute of Fine Chemicals, College of Chemistry and Molecular Engineering, East China University of Science and Technology, 130 Meilong Rd., Shanghai 200237, China

[b] The State Key Laboratory of Bioreactor Engineering, Key Laboratory for Ultrafine Materials of Ministry of Education, East China University of Science and Technology, Shanghai, China

ARTICLE INFO

Article history:
Received 24 April 2017
Received in revised form 5 June 2017
Accepted 5 June 2017
Available online 10 June 2017

Keywords:
Diketopyrrolopyrrole
Fluorescent probes
Colorimetric
Ratiometric
SO_2 derivatives
Mitochondrial

ABSTRACT

Two new fluorescent probes (**DPP-FI**/**DPP-BI**) based on diketopyrrolopyrrole (DPP) were designed and synthesized for colorimetric and ratiometric detection of SO_2 derivatives. Both of them displayed obvious ratiometric changes with about 21 folds of fluorescent ratio transformation from red to yellow upon treating with bisulfite to interrupt the π-conjugation of probes. In addition, the calculated detection limit of **DPP-FI** and **DPP-BI** was down to 2.34×10^{-6} M and 1.73×10^{-6} M towards HSO_3^-, respectively. Besides, **DPP-FI**/**DPP-BI** showed outstanding selectivity toward HSO_3^-/SO_3^{2-} over other nucleophilic anions. More importantly, these two probes could successfully detect mitochondrial HSO_3^- in HepG2 cells, which is to our knowledge the first example using DPP as colorimetric and ratiometric fluorescent probes to detect small molecules in organelles.

1. Introduction

Sulfur dioxide (SO_2), a kind of industrial waste, has been considered as toxic environmental pollutant. Recent studies have demonstrated that SO_2 even at low concentrations in the environment will cause not only some respiratory diseases, but also induced lung cancer [1], cardiovascular disease [2,3], and nervous system diseases (such as migraine, stroke, and brain tumors) [4–6]. Endogenous biological SO_2 mainly generated enzymatically in the mitochondria of cells, which was as an oxidation product from hydrogen sulfide [7,8] and some other sulphur-containing amino acids [9], can regulate the structure and function of cardiovascular, such as lowering blood pressure and vasodilation [10]. However, it also destroys the enzyme activity once exceed normal concentrations [11] (16.77 ± 8.24 μmol/L in plasma), thus affecting human metabolism [12]. Therefore, it is important to develop a reliable assay method for detecting SO_2 and its derivatives in living systems. As the mainly exists form of SO_2 in living cells, HSO_3^-/SO_3^{2-} has been widely concerned [13].

To date, a variety of disparate approaches have been applied to SO_2 derivatives determination, including spectrophotometry [14,15], electro-chemistry [16,17], chromatography [18,19], chemiluminescence [20,21], capillary electrophoresis [22] and enzymatic techniques [23]. However, these methods are usually unsuitable for routine analysis due to the requirement of tedious sample and reagent preparation or complicated instruments. Therefore, new techniques for accurate detection of HSO_3^-/SO_3^{2-} levels with good selectivity and high sensitivity are in high demand to provide valuable information on the functions of HSO_3^-/SO_3^{2-} in biology.

Fluorescent probes provided an indispensable real tool for real-time sensing and visualization of some biological species because of its high sensitivity, non-invasiveness, high temporal and spatial resolution. Up to now, several fluorescent probes for HSO_3^-/SO_3^{2-} have been reported based on HSO_3^- nucleophilic reaction with aldehydes [24–26], coordinative interactions [27,28] and the selective deprotection of levulinate [29]. But they have some disadvantages such as too long response time (5min–10 h), unsatisfactory detection limit. And also suffered interference from hydrogen sulfide (H_2S), cysteine (Cys), homocysteine (Hcy), glutathione (GSH), protease or esterase. Besides, these probes display changes only in the fluorescence emission intensity, thereby being subjected to environmental conditions and instrumental efficiency.

* Corresponding author.
E-mail address: jlhua@ecust.edu.cn (J. Hua).

http://dx.doi.org/10.1016/j.jphotochem.2017.06.007
1010-6030/

Diketopyrrolopyrrole (DPP) was a robust chromophore and had been extensively used as organic photovoltaics [30–32], semiconductors [33–35] and two-photon absorption materials [36,37]. Furthermore, on the one hand, unmodified DPP emits green fluorescence but it can reach the near-infrared region after modification. On the other hand, compared with other commercial dyes, the structure of DPP has a certain rigidity. As a result, it improves the light stability under high power excited source and ensuring quantum efficiency at the same time, which makes it the potential material of chemical and biological probes. Therefore, since the first example using DPP as fluorescent probe reported by our group [38], it has been widely developed on reaction-based fluorescent probes by our group [39,40] and other groups [41–45]. However, DPP was rarely reported in the field of organelles-targeted [46], especially none of it has been applied to detect small molecules in organelles. Recently, Zhang's group has reported a new fluorescent probe for sulphite detection based on DPP derivative [47], but it takes too long time to response, easily being affected by the auto-fluorescence after nucleophilic addition of sulfite, and had not been applied in living cells imaging. Therefore, two new probes for HSO_3^-/SO_3^{2-} were designed and synthesized in our present work, in which DPP was used as the fluorophore, and the α,β-unsaturated structure between DPP and indolium moiety was designed to detect HSO_3^-/SO_3^{2-} (Scheme 1). Meanwhile, the introduced indolium improved the water solubility, and made it a potential mitochondria-targeted probe due to its positively charged [48,49]. Results indicated that these two probes had good biocompatibility, selectivity and good competition for sulfite over other some anions and biothiols just within 4 min. And their ratiometric properties gave them much lower detection limit, less auto-fluorescence interference and higher accuracy. In addition, these two probes have been demonstrated to realize mitochondria-localized and be used for direct visualization of HSO_3^-/SO_3^{2-} in living cells.

2. Experimental section

2.1. Reagents and measurements

Unless otherwise stated, reagents were commercially obtained and used without further purification. Reactions were monitored by TLC. Flash chromatography separations were carried out using silica gel (200–300 mesh). Dry *N,N*-Dimethylformamide (DMF) were also commercially obtained and without further purification.

^1H and ^{13}C NMR spectra were recorded on a Bruker AM 400 MHz spectrometer using $CDCl_3$ or DMSO-d_6 as solvent and tetramethylsilane (TMS) as the internal reference. Absorption spectra were measured with a Varian Cary 500 UV–vis spectrophotometer. Fluorescence measurements were collected using a Horiba Fluoromax − 4 fluorescence spectrometer.

2.2. Calculation of LOD

Plotting the ratio of $\mathbf{I_1/I_2}$($\mathbf{I_1}$ and $\mathbf{I_2}$ refers to value of the corresponding emission maxima before and after reaction with HSO_3^-) as a function of HSO_3^- concentration for determination of the limit of detection (LOD). LOD were calculated by the equation 3δ/slope (δ is a standard deviation of the measured value of the emission maxima of blank solution for seven times).

2.3. Determination of fluorescence quantum yields

The relative fluorescence quantum yields of **DPP-FI/DPP-BI** were respectively determined in ethanol before and after the reaction with $NaHSO_3$. The fluorescence of Rhodamine B ($\Phi_f = 0.97$) in ethanol was chosen as a standard [50].

2.4. Synthesis

2.4.1. Synthesis of compound *1*

A mixture of ethyl benzoylacetate (4.81 g, 25.0 mmol), K_2CO_3 (3.59 g, 26.0 mmol), KI (0.53 g, 3.2 mmol) and ethyl bromide (4.34 g, 26 mmol) in acetone (20 mL) and 1,2-dimethoxyethane (10 mL) was stirred at 75 °C for 24 h, then cooled to room temperature and filtered. The filter was collected and acetone was removed via rotatory evaporation. The residue was diluted with CH_2Cl_2 and washed with water. The organic layer was dried with anhydrous $MgSO_4$ and the solvent was removed via rotatory evaporation to give yellow liquid crude product. The crude product and ammonium acetate (18.69 g, 242.5 mmol) were dissolved in 50 mL of acetic acid, and then the solution was stirred under argon protection at 120 °C for 8 h. After cooling to room temperature, the mixture was poured into ice water. The precipitate was collected and dried under vacuum to give **1** as gray solid (3.46 g, 60.49%).

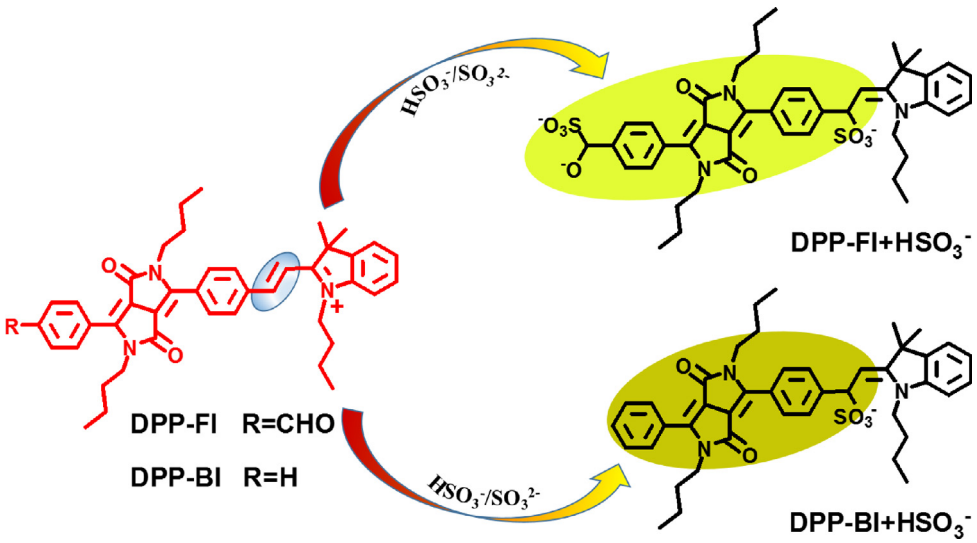

Scheme 1. Chemical structure of probe **DPP-FI/DPP-BI** and reaction mechanism of probe **DPP-FI/DPP-BI** with HSO_3^-/SO_3^{2-}.

*2.4.2. Synthesis of compound **2***

Sodium (180.0 mg, 7.5 mmol) was added in t-amyl alcohol (20 mL) at 50 °C, the mixture was heated to 100 °C until the sodium disappeared completely. Then the solution was cooled to 50 °C, compound 1 (462 mg, 2.0 mmol) and 4-(1,3-dioxolan-2-yl) benzonitrile (525 mg, 3.0 mmol) was added. Subsequently, the resulting suspension was stirred at 100 °C overnight under the protection of an argon atmosphere, and cooled to room temperature. The mixture was poured into a mixture of hydrochloric acid and methanol. The precipitate was filtered and washed with water and methanol, dark-red solid was obtained after dried under vacuum (300 mg, 41.63%). The product was used without further purification.

*2.4.3. Synthesis of compound **3***

Sodium (4.00 g, 174 mmol) was added in t-amyl alcohol (100 mL) at 50 °C, the mixture was heated to 100 °C until the sodium disappeared completely. Then the solution was cooled to 50 °C, 4-(1,3-dioxolan-2-yl) benzonitrile (13.8 g, 78.86 mmol) was added, diisopropyl succinate (8.07 mL, 39.43 mmol) in t-amyl alcohol (30 mL) was added dropwise under the protection of an argon atmosphere. Subsequently, the resulting suspension was stirred at 100 °C overnight, and cooled to room temperature. The mixture was poured into a mixture of hydrochloric acid and methanol. The precipitate was filtered and washed with water and methanol, dark-red solid was obtained after dried under vacuum (5.96 g, 35%). The product was used without further purification.

*2.4.4. Synthesis of compound **4***

Compound **3** (864 mg, 2.0 mmol), NaH (200 mg, 8.3 mmol) were dissolved in dry DMF (20 mL), the mixture was then stirred at 0 °C for 1 h under argon protection. Then the reaction mixture was warmed to room temperature and *n*-iodobutane (0.91 mL, 8.0 mmol) was added dropwise. The mixture was kept at 100 °C for 8 h before being allowed to cool room temperature. The mixture was poured into ice water, the precipitate was collected and dried under vacuum to give **4** as an orange solid (505 g, 46.28%) which was used directly without further purification.

*2.4.5. Synthesis of compound **5***

From **2** (720.72 mg, 2.0 mmol) and *n*-iodobutane (0.91 mL, 8.0 mmol), the mixture was poured into ice water, the precipitate was collected and dried under vacuum to give **5** as an orange solid (380 mg, 40.25%) which was used directly without further purification.

*2.4.6. Synthesis and characterization of compound **6***

Compound **4** (400 mg, 0.73 mmol), THF (20 mL), and HCl (2 M, 10 mL) were added into a two-necked flask, the reaction mixture was stirred for 2 h at 60 °C, then cooled to room temperature and saturated brines (30 mL) was added, the organic layer was collected and dried over Na_2SO_4. Removal of the solvent under vacuum and the crude product was purified by column chromatography (silica gel; DCM/ethyl acetate, 30/1, v/v) to provide the corresponding pure product **6** (274 mg, 85.62%) as an orange solid. ^{1}H NMR (400 MHz, $CDCl_3$) δ (ppm): 10.03 (s, 2H), 7.98 (d, *J* = 8.4 Hz, 4H), 7.92 (d, *J* = 8.4 Hz, 4H), 3.71 (t, *J* = 8.4 Hz, 4H), 1.52-1.46 (m, 4H), 1.24-1.15 (m, 4H), 0.77 (t, *J* = 7.3 Hz, 6H). ^{13}C NMR (100 MHz, $CDCl_3$), *δ* (ppm): 190.21, 161.23, 146.60, 136.62, 132.25, 128.96, 128.26, 110.01, 40.73, 30.47, 18.90, 12.53. HRMS (ESI, *m*/*z*): $[M+H]^+$ calcd. for $C_{28}H_{29}N_2O_4^+$ 457.2127, found 457.2130.

*2.4.7. Synthesis and characterization of compound **7***

From **5** (120 mg, 0.29 mmol) by treated with HCl, column chromatography (eluent: DCM/ethyl acetate, 40/1, v/v) gave **9** (149.22 mg, 84.89% yield) as an orange solid. ^{1}H NMR (400 MHz, $CDCl_3$) δ (ppm): 10.09 (s, 1H), 8.04 (d, *J* = 8.3 Hz, 2H), 7.98 (d, *J* = 8.3 Hz, 2H), 7.82 (dd, *J* = 6.5, 3.1 Hz, 2H), 7.56 – 7.52 (m, 3H), 3.77 (t, *J* = 8.3 Hz, 4H), 1.60 – 1.53 (m, 4H), 1.30 – 1.25 (m, 4H), 0.84 (td, *J* = 4.1 Hz, 4.1 Hz, 6H). ^{13}C NMR (100 MHz, $CDCl_3$), δ (ppm): 191.31, 162.66, 162.37, 150.09, 146.08, 137.43, 133.70, 131.49, 130.01, 129.21, 128.96, 128.75, 127.93, 111.21, 109.70, 41.74, 31.58, 31.49, 19.96, 13.57. HRMS (ESI, *m*/*z*): $[M+H]^+$ calcd. for $C_{27}H_{29}N_2O_3^+$ 429.2178, found 429.2193.

*2.4.8. Synthesis and characterization of compound **DPP-FI***

Compound **6** (218 mg, 0.5 mmol), 1-butyl-2,3,3-trimethyl-3*H*-indolium (108 mg, 0.5 mmol) and three drops of piperidine were dissolved in acetonitrile. The reaction mixture was stirred at 80 °C for 7 h under the protection of an argon atmosphere. Then the mixture was cooled to room temperature, and the reaction solvent was evaporated under vacuum, then the residue was purified by flash column chromatography on silica gel (DCM/ethanol, 30/1, v/v) to provide the corresponding pure product **DPP-FI** (110 mg, 33.64%) as a dark-red solid. ^{1}H NMR (400 MHz, DMSO-d_6) δ (ppm): 10.13 (s, 1H), 8.55 (d, *J* = 16.4 Hz, 1H), 8.45 (d, *J* = 8.5 Hz, 2H), 8.15-8.05 (m, 6H), 8.03 – 7.99 (m, 1H), 7.96 – 7.93 (m, 1H), 7.87 (d, *J* = 16.4 Hz, 1H), 7.69 – 7.65 (m, 2H), 4.78 (t, *J* = 7.2 Hz, 2H), 3.79 (dt, *J* = 15.9, 7.5 Hz, 4H), 1.85 (s, 6H), 1.49 – 1.37 (m, 8H), 1.19 – 1.13 (m, 4H), 0.95 (t, *J* = 7.3 Hz, 3H), 0.76 (dd, *J* = 15.9, 7.4 Hz, 6H). ^{13}C NMR (100 MHz, DMSO-d_6), *δ* (ppm): 192.65, 181.81, 161.31, 147.39, 144.20, 140.67, 137.45, 132.69, 130.81, 129.74, 129.30, 129.22, 129.16, 123.18, 115.72, 114.43, 110.08, 110.04, 52.55, 30.72, 30.67, 25.50, 19.28, 19.21, 13.70, 13.37, 13.29. HRMS (ESI, *m*/*z*): $[M+H]^+$ calcd. for $C_{43}H_{48}N_3O_3^+$ 654.3696, found 654.3687.

*2.4.9. Synthesis and characterization of compound **DPP-BI***

From **7** (100 mg, 0.24 mmol) and 1-butyl-2,3,3-trimethyl-3*H*-indolium (51.84 mg, 0.24 mmol), column chromatography eluent: dichloromethane/ethanol (40:1, v/v) gave **DPP-BI** (94.24 mg, 64.8% yield) as a dark-red solid. ^{1}H NMR (400 MHz, DMSO-d_6) δ(ppm): ^{1}H NMR (400 MHz, DMSO-d_6) δ (ppm): 8.55 (d, *J* = 15.5 Hz, 1H), 8.45 (d, *J* = 7.2 Hz, 2H), 8.07 (d, *J* = 7.6 Hz, 2H), 8.04 – 7.93 (m, 2H), 7.87 (dd, *J* = 7.7 Hz, 3.9 Hz, 3H), 7.65 (d, *J* = 17.7 Hz, 5H), 4.78 (t, *J* = 8.4 Hz, 2H), 3.84 – 3.72 (m, 4H), 1.85 (s, 6H), 1.48 – 1.39 (m, 8H), 1.18 – 1.12 (m, 4H), 0.95 (t, *J* = 4.2 Hz, 3H), 0.77 (t, *J* = 8.4 Hz, 6H). ^{13}C NMR (100 MHz, DMSO-d_6), δ (ppm): 181.79, 161.53, 161.36, 148.96, 146.14, 144.17, 140.67, 136.59, 130.80,129.08, 128.95, 128.60, 127.55, 123.17, 115.69, 114.28, 110.02, 108.84, 52.52, 30.75, 30.64, 25.50, 19.27, 19.22,13.69, 13.37, 13.29. HRMS (ESI, *m*/*z*): $[M+H]^+$ calcd. for $C_{42}H_{48}N_3O_2^+$ 626.3747, found 626.3749.

3. Results and discussion

3.1. Molecular design and synthesis

It is well known that α,β-unsaturated indolium dyes possess similar structure to acrylonitrile which could rapidly and quantitatively response to HSO_3^-/SO_3^{2-} [51,52], and this type of dye has been demonstrated to be inert to biothiols, such as Cys and GSH [53–55]. Meanwhile, after nucleophilic addition of HSO_3^-/SO_3^{2-} toward the unsaturated bonds, π-conjugation and ICT process was broken and blocked, resulting in two well-separated emission peaks which would enable the ratiometric sensing of HSO_3^-/SO_3^{2-}. In order to obtain the sensitive and selective fluorescent probes with ratiometric and colorimetric for the detection of SO_2 derivatives, **DPP-FI** was designed and synthesized (Scheme 2) in which the aldehyde group could affect the nucleophilic addition of HSO_3^- and the emission wavelength. As a contrast, **DPP-BI** without aldehyde group was also synthesized (Scheme 2). For these two probes, the introduction of indolium group would be beneficial to improve the water solubility of the

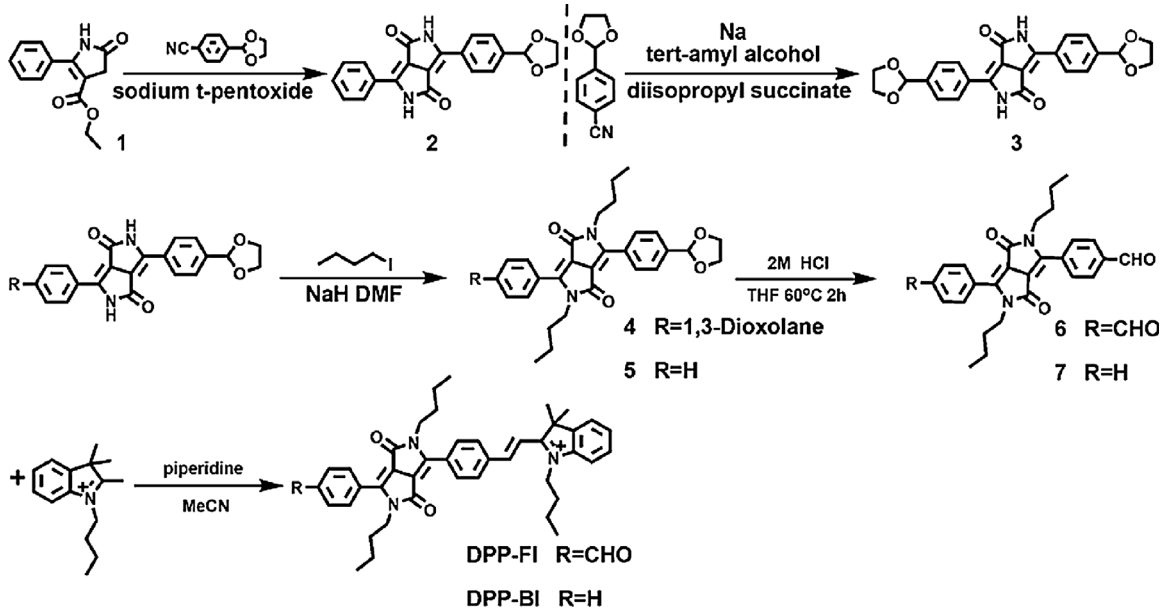

Scheme 2. Synthesis of the target **DPP-FI** and **DPP-BI**.

molecule in some degree, additionally, the indolium moiety as a mitochondria-targeted functional group could realize the cellular organelle localization.

The synthesis of targets **DPP-FI** and **DPP-BI** are shown in Scheme 2. In the first step, the two different DPP cores were synthesized by one step reaction of cyclization to form (compounds **2** and **3**) from compound 1 and 4-(1,3-dioxolan-2-yl) benzonitrile, respectively, then 1-iodobutane was attached to the core of DPP with the catalysis of NaH to produce the alkyl DPP intermediates **4** and **5**. Then deprotection reactions were conducted by treated with HCl to provide corresponding compounds **6** and **7**, which were finally react with indolium dyes to produce the desirable compounds **DPP-FI** and **DPP-BI** according to Knoevenagel reaction. All of the structures of new compounds were well-characterized by ^{1}H NMR, ^{13}C NMR, and HRMS (ESI).

3.2. Characterization of DPP-FI and DPP-BI for SO_3^{2-}/HSO_3^- recognition

UV-vis absorption spectra properties were studied firstly in aqueous solution (PBS: DMSO = 7:3, pH = 7.4). The changes of the absorption spectra in the absence and presence of HSO_3^- (0–20equiv.) were displayed in Fig. 1. The probe **DPP-FI** showed an absorption band at 520 nm ($\varepsilon = 1.43 \times 10^4\,M^{-1}cm^{-1}$), but decreased when HSO_3^- was added to the solution, while an absorption band at 480 nm ($\varepsilon = 1.25 \times 10^4\,M^{-1}cm^{-1}$) developed, which was visible to the naked eye with a clear color change from pink to yellow (Fig. 1a). Similar to **DPP-FI**, **DPP-BI** demonstrated same changes that absorbance shifted from 505 nm ($\varepsilon = 2.10 \times 10^4\,M^{-1}cm^{-1}$) to 475 nm ($\varepsilon = 1.83 \times 10^4\,M^{-1}cm^{-1}$) after addition with HSO_3^- (Fig. 1d).

The emission spectra and fluorescence titration experiments of probe **DPP-FI** and **DPP-BI** with HSO_3^- were then recorded in aqueous solution (PBS: DMSO = 7:3, pH = 7.4) (Fig. 1). The free probe **DPP-FI** displayed weak red fluorescence. With titration of HSO_3^- from 0 to 20 equiv. to the solution, the probe was converted efficiently to an additive product. And an obvious decrease in fluorescence intensity at 720 nm ($\Phi_f = 0.12$) was observed; Meanwhile, the fluorescence intensity of the emission band at 545 nm ($\Phi_f = 0.18$) increased significantly. Compared with **DPP-FI**, in the presence of HSO_3^-, the emission band at 670 nm ($\Phi_f = 0.43$) of **DPP-BI** decreased and a new emission band at 535 nm ($\Phi_f = 0.27$) developed, it is obvious that **DPP-BI** showed slight blue shift of fluorescent emission both before and after react with HSO_3^-, which may ascribe to the weaker electron-withdrawing ability of hydrogen atom towards aldehyde group. The distinct emission spectral shift (about 145 nm) of **DPP-FI** and **DPP-BI** showed that they were favorable for ratiometric fluorescence detection. In addition, the time-dependent fluorescence responses were also detected with 10 equiv. of HSO_3^- from 0 to 8 min, and the results showed that the reaction was almost completed within 4 min (Fig. S1).

3.3. Selectivity towards different species

To investigate the selectivity of **DPP-FI** and **DPP-BI** towards HSO_3^-/SO_3^{2-}, the emission intensity ratio of **DPP-FI** and **DPP-BI** were measured toward various species. As shown in Fig. 2, HSO_3^-/SO_3^{2-} exclusively produced a dramatic increment in the emission intensity ratio. The responsiveness of **DPP-FI** and **DPP-BI** to HSO_3^-/SO_3^{2-} were approximately 21-fold versus other species. The other nucleophilic anions (F^-, Cl^-, Br^-, I^-, HCO_3^-, AcO^-, NO_3^-, $S_2O_3^{2-}$, SO_4^{2-}, HSO_4^-, PO_4^{3-}, HPO_4^{2-}, $H_2PO_4^-$, Citrate, HS^-), oxidizing reagents (H_2O_2, ClO^-) and three sulphur-containing amino acids (Hcy, Cys, GSH) did not cause the ratiometric change. The emission intensity ratio of these species were almost an order of magnitude lower than that generated by HSO_3^-/SO_3^{2-}, despite their 5-fold concentrations versus HSO_3^-/SO_3^{2-}. All above considered, **DPP-FI/DPP-BI** showed outstanding selectivity towards HSO_3^-/SO_3^{2-} over other common biological species.

3.4. Effect of pH on the fluorescence of DPP-FI and DPP-BI

In mitochondria, the internal environment pH was about 8.05 ± 0.11, so the probe should remain stable in slightly alkaline environment with no fluorescence response. Firstly, we investigated the influence of pH on the fluorescent properties of **DPP-FI/DPP-BI** in a wide range of pH values in aqueous solution (PBS: DMSO = 7:3) (Fig. 3). What we can see from the fluorescent ratio of **DPP-FI/DPP-BI** is that these two probes exhibited a weak emission band with a maximum at 545 nm and 535 nm respectively, thus increased sharply after addition of HSO_3^-. Hence, the stable fluorescence of

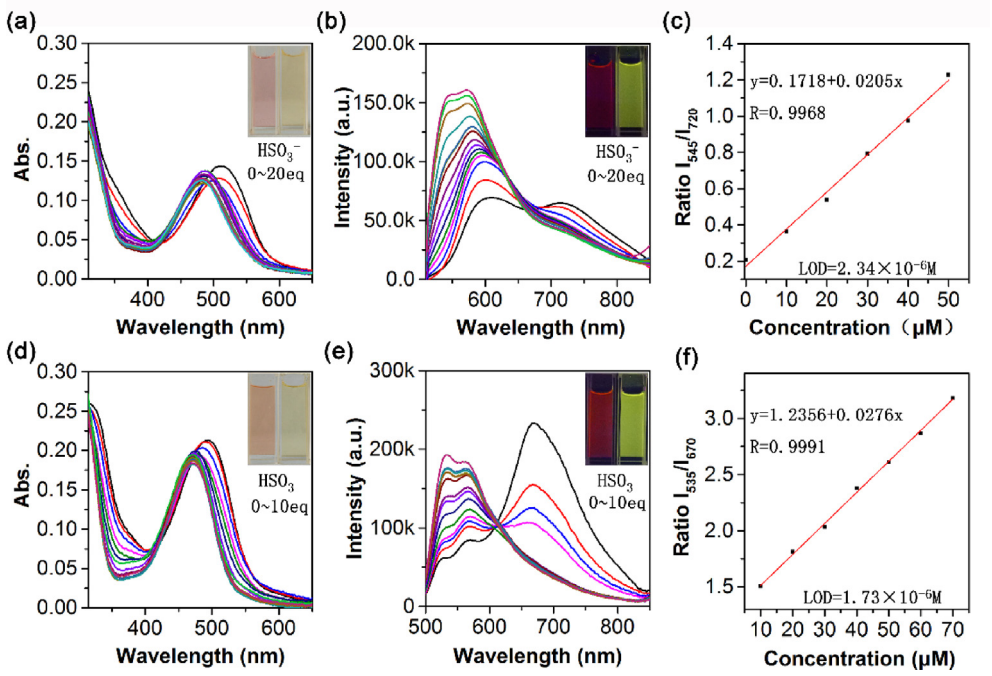

Fig. 1. UV-vis absorption spectra of (a) **DPP-FI** (10 μM) and (d) **DPP-BI** (10 μM) with different equiv. (from 0 to 20 eq.) HSO_3^- in DMSO-buffer solution (PBS: DMSO = 7:3, v/v, pH = 7.4) at 37 °C for 4 min. Insert: photograph showing the visual color of **DPP-FI** and **DPP-BI** when treated without (left) or with (right) HSO_3^- under visible light. Fluorescence spectra of (b) **DPP-FI** (10 μM) and (e) **DPP-BI** (10 μM) with different equiv. (from 0 to 10 eq.) HSO_3^- in DMSO-buffer solution (PBS: DMSO = 7:3, v/v, pH = 7.4) at 37 °C for 4 min. λ_{ex} = 480 nm and 475 nm respectively. Insert: photograph showing the visual fluorescence color of **DPP-FI** and **DPP-BI** when treated without (left) or with (right) HSO_3^- under a 365 nm UV lamp. (c) Linear relationship between the fluorescence ratio (I_{545}/I_{720}) changes and the determination of the limit of detection (LOD) of **DPP-FI**. (f) Linear relationship between the fluorescence ratio (I_{535}/I_{670}) changes and the determination of the limit of detection (LOD) of **DPP-BI**.

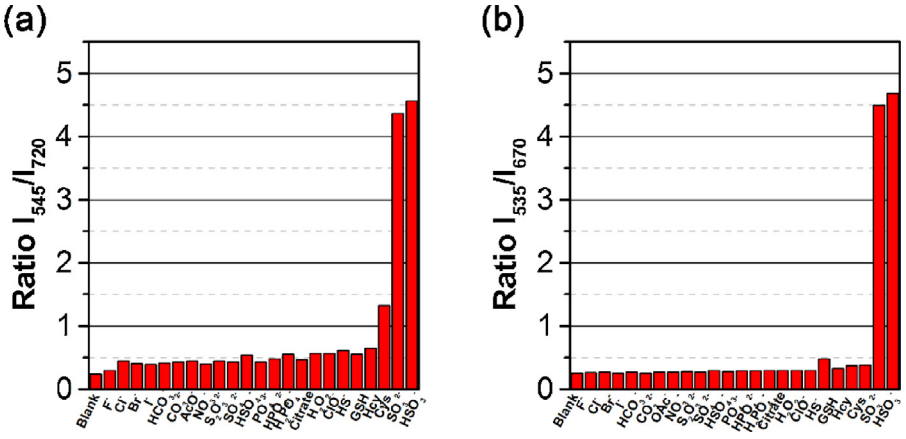

Fig. 2. (a) Fluorescence ratio (I_{545}/I_{720}) of **DPP-FI** (10 μM) and (b) ratio variation of I_{535}/I_{670} of **DPP-BI** in 10 equiv. HSO_3^-/SO_3^{2-} and 50 equiv. various other additives in DMSO-buffer solution (PBS: DMSO = 7:3, v/v, pH = 7.4). λ_{ex} = 480 nm and 475 nm respectively.

DPP-FI and **DPP-BI** in the pH range 3.0–9.0 can provide its application in monitoring intracellular SO_2 derivatives in living cells.

3.5. Detection mechanism in sensing HSO_3^-

To further explain the reaction pathway, ^{1}H NMR and MS titrations were carried out in DMSO-d_6. The partial ^{1}H NMR spectra of **DPP-FI** before and after treatment with different equiv. of HSO_3^- is shown in Fig. 4. When 0.5 equiv. HSO_3^- (dissolved in D_2O) were added, the resonance signal corresponding to the vinylic proton H_b at 8.55 ppm (doublet) and H_c at 7.87 ppm (doublet) significantly decreased because of the nucleophilic attack of HSO_3^-, while the proton signals at 10.13 ppm was assigned to H_a in **DPP-FI** was retained (Fig. 4 middle row). After addition of 5 equiv. HSO_3^-, the proton signal of δ 10.13 ppm was shifted to 5.10 ppm attributed to the nucleophilic addition to the formyl group, and the chemical shift of H_b and H_c shifted to 5.00 and 4.92 ppm completely, meanwhile, a new peak at 3.54 ppm (triplet, H_d') appeared due to the disappeared positively-charged of indolium group (Fig. 4 under row). Furthermore, an MS titration was also performed to confirm the reaction mechanism (Fig. S6 and S7). Similar results were also obtained for **DPP-BI** according to its ^{1}H NMR and MS titrations (Fig. S2 and S8). All these results indicate that bisulfite ion attack the α, β-unsaturated bond between DPP and indolium moiety first, then nucleophilic addition to the extra formyl group if exist.

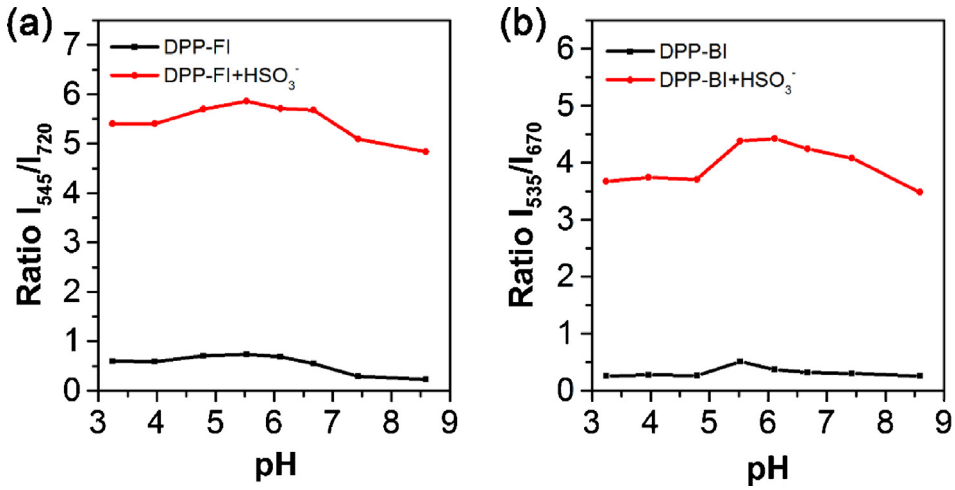

Fig. 3. (a) Fluorescence ratio (I_{545}/I_{720}) of **DPP-FI** (10 μM) and (b) ratio (I_{535}/I_{670}) of **DPP-BI** (10 μM) before (black squares) and after (red dots) the addition of 100 μM HSO_3^- for 4 min at different pH values. λ_{ex} = 480 nm and 475 nm respectively. (For interpretation of the references to colour in this figure legend, the reader is referred to the web version of this article.)

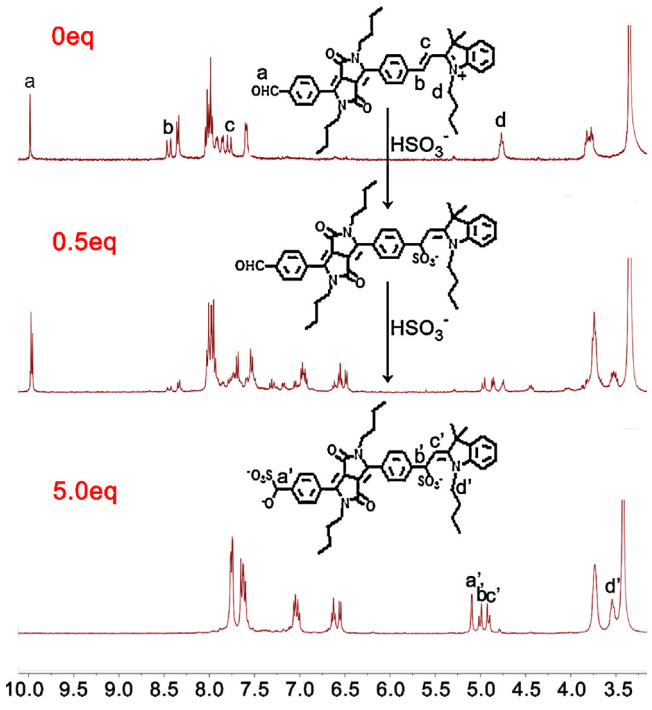

Fig. 4. ^{1}H NMR spectra titration of **DPP-FI** with different equivalent HSO_3^- in DMSO-d_6.

3.6. Intracellular detection

The cytotoxicity of two probes was evaluated by MTT with the probe concentration at 10 μM and HSO_3^- concentration at 50 μM, and the results were shown in Fig. S3. The results demonstrated that **DPP-FI** and **DPP-BI** showed little cytotoxicity for long period incubation and should be safe when used for imaging.

To prove the cellular organelle localization of **DPP-FI/DPP-BI** with a positively-charged of indolium moiety as a mitochondria-targeted group, a commercially available mitochondrial dye (Mito Tracker Red CMXRos), was employed for a co-localization study. HepG2 cells were co-incubated with **DPP-FI** (10 μM) and Mito Tracker Red CMXRos (500 nM) at 37 °C for 30 min, then treated with 50 μM HSO_3^-. As shown in Fig. 5b, a clear mitochondria profile with strong red fluorescence was observed from the red channel, which was ascribed to Mito Tracker Red CMXRos. A similar mitochondria profile with green fluorescence was obtained after incubation with **DPP-FI** and HSO_3^- (Fig. 5a). From Fig. 5e, we can see that the changes in the intensity profiles of linear regions of interest (ROIs) (**DPP-FI** and Mito Tracker Red CMXRos co-staining) were synchronous, and the fluorescence signals of the probe overlaid well with those of Mito Tracker Red CMXRos. Furthermore, co-localization was quantified using the Pearson's co-localization coefficient. The intensity of the correlation plot (Fig. 5f), which described the distribution between the green channel (Fig. 5a) and red channel (Fig. 5b), revealed a high co-localization coefficient (0.84), Similar experiments were also conducted for **DPP-BI**, and it showed same satisfactory results (Fig. S4), all these proved that **DPP-FI/DPP-BI** was site specifically internalized in mitochondria and it could be used to detect mitochondrial SO_2 derivatives in cancer cells.

Next, we attempted to apply **DPP-FI/DPP-BI** to ratiometric fluorescence imaging of SO_2 derivatives in vivo systems. As shown in Fig. 6, we incubated 10 μM **DPP-FI** with HepG2 cells for 30 min at 37 °C in PBS, and confocal laser scanning microscopy was carried out in living cells. On excitation at 480 nm, **DPP-FI** exhibited red fluorescence in the red channel from 690 to 750 nm, but negligible through green channel from 525 to 575 nm on excitation at 480 nm. After addition of the HSO_3^- to **DPP-FI** loaded HepG2 cells for 30 min incubation, **DPP-FI** stained cells exhibited distinct changes of ratiometric fluorescence responses generated from green channel and red channel in living cells, thus leading to a significant increase in fluorescence ratio (from 0.21 to 4.51, about 21-fold). For **DPP-BI**, similar experiments were also conducted, and we obtained similar fluorescence changes in living cells (Fig. S5). All these results confirmed that both **DPP-FI** and **DPP-BI** could be used for ratiometric fluorescence imaging of mitochondrial SO_2 derivatives in living cells.

4. Conclusions

In summary, two new DPP-based derivatives (**DPP-FI/DPP-BI**) for the imaging of mitochondrial SO_2 derivatives in living cells have been developed. The ratiometric and colormetric sensing is realized by broken the π-conjugation structure due to nucleophilic attack of HSO_3^-, which were determined by ^{1}H NMR and MS titration analysis. Both probes could detect SO_2 derivatives with

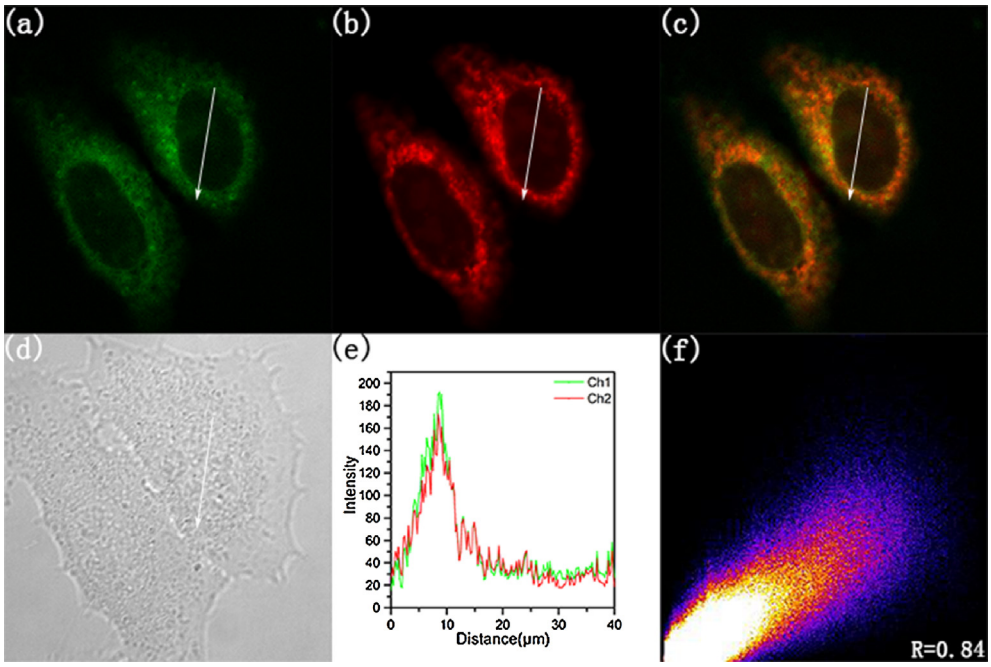

Fig. 5. Confocal fluorescence images of HepG2 cells stained with (a) 10 μM **DPP-FI** (green channel: λ_{ex} = 480 nm, λ_{em} = 525–575 nm) at 37 °C for 30 min then added 50 μM $NaHSO_3$ solution for 30 min and (b) 500 nM MitoTracker Red CMXRos (red channel: λ_{ex} = 579 nm, λ_{em} = 570–630 nm) at 37 °C for 30 min; (c) Merged image of (a) and (b); (d) Bright field image; (e) Intensity profiles of regions of interest (ROI) across HepG2 cells. Green lines represent the intensity of the probe **DPP-FI** treated with HSO_3^- and red lines represent the intensity of Mito Tracker Red CMXRos; (f) Correlation plot of MitoTracker Red CMXRos and **DPP-FI** intensities. (For interpretation of the references to colour in this figure legend, the reader is referred to the web version of this article.)

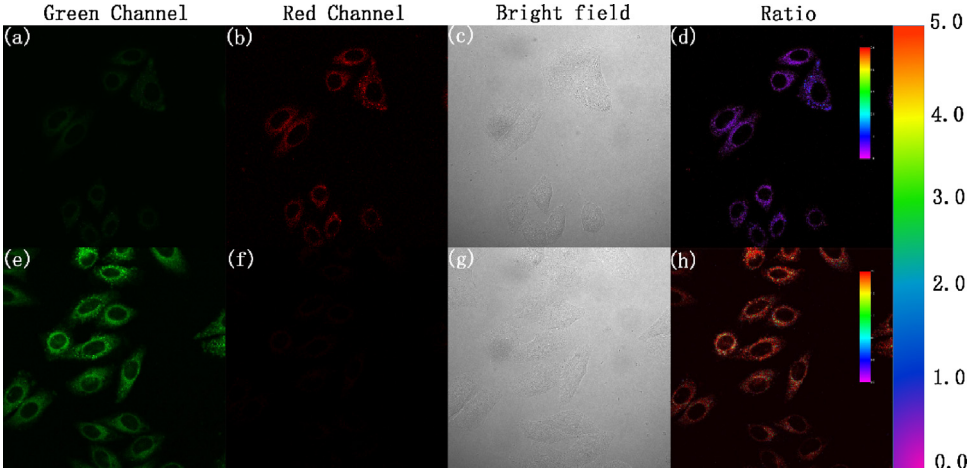

Fig. 6. (a) Fluorescence imaging of HepG2 cells incubated with **DPP-FI** (10 μM) from the green channel; (b) Fluorescence imaging of (a) from the red channel; (c) Bright field of (a). (d) Fluorescence intensity ratio signals of (a) and (b); (e) Fluorescence imaging of HepG2 cells incubated with **DPP-FI** (10 μM) for 30 min and further incubated with $NaHSO_3$ (50 μM) for 30 min from the green channel; (f) Fluorescence imaging of (e) from the red channel; (g) Bright field of (e). (h) Fluorescence intensity ratio signals of (e) and (f). Green channel: λ_{ex} = 480 nm, λ_{em} = 525–575 nm, Red channel: λ_{ex} = 480 nm, λ_{em} = 690–750 nm (For interpretation of the references to colour in this figure legend, the reader is referred to the web version of this article.)

excellent sensitivity and selectivity. Probes **DPP-FI/DPP-BI** displayed a significant blue shift (about 145 nm) in its fluorescence spectra in the presence of SO_2 derivatives within few minutes (4 min). More importantly, Co-staining experiments of **DPP-FI/DPP-BI** and Mito Tracker Red CMXRos (co-localization coefficient: 0.84 and 0.81) revealed that **DPP-FI/DPP-BI** were predominantly present in mitochondria, which is to our knowledge the first example employing DPP probes **DPP-FI/DPP-BI** for imaging of mitochondrial SO_2 derivatives in HepG2 cells. Hence, we expect this research paves a significant way for designing more DPP-based colorimetric and ratiometric fluorescent probes with effective sensing capability and specific organelle localization for biological applications.

Acknowledgements

For financial support of this research, we thank NSFC/China (21372082, 21421004 and 21572062), the National Basic Research 973 Program (2013CB733700), the Fundamental Research Funds for the Central Universities (222201717003) and the Programme of Introducing Talents of Discipline to Universities (B16017).

Appendix A. Supplementary data

Supplementary data associated with this article can be found, in the online version, at http://dx.doi.org/10.1016/j.jphotochem.2017.06.007.

References

[1] K. Ohyamaa, T. Itob, M. Kanisawa, The roles of diesel exhaust particle extracts and the promotive effects of NO_2 and/or SO_2 exposure on rat lung tumorigenesis, Cancer Lett. 139 (1999) 189–197.
[2] J. Li, R. Li, Z. Meng, Sulfur dioxide upregulates the aortic nitric oxide pathway in rats, Eur. J. Pharmacol. 645 (2010) 143–150.
[3] X.B. Wang, H.F. Jin, C.S. Tang, J.B. Du, The biological effect of endogenous sulfur dioxide in the cardiovascular system, Eur. J. Pharmacol. 675 (2011) 1–6.
[4] G. Li, N. Sang, Delayed rectifier potassium channels are involved in SO_2 derivative-induced hippocampal neuronal injury, Ecotoxicol. Environ. Saf. 72 (2009) 236–241.
[5] N. Sang, Y. Yun, H. Li, L. Hou, M. Han, G. Li, SO_2 inhalation contributes to the development and progression of ischemic stroke in the brain, Toxicol. Sci. 114 (2010) 226–236.
[6] S.S. Tsai, W.B. Goggins, H.F. Chiu, C.Y. Yang, Evidence for an association between air pollution and daily stroke admissions in Kaohsiung, Taiwan, Stroke 34 (2003) 2612–2616.
[7] S. Du, H. Jin, D. Bu, X. Zhao, B. Geng, C. Tang, J. Du, Endogenously generated sulfur dioxide and its vasorelaxant effect in rats, Acta Pharmacol. Sin. 29 (2008) 923–930.
[8] L. Luo, S. Chen, H. Jin, C. Tang, J. Du, Endogenous generation of sulfur dioxide in rat tissues, Biochem. Biophys. Res. Commun. 415 (2011) 61–67.
[9] M.H. Stipanuk, I. Ueki, Dealing with methionine/homocysteine sulfur: cysteine metabolism to taurine and inorganic sulfur, J. Inherit. Metab. Dis. 34 (2011) 17–32.
[10] Z. Meng, Z. Yang, J. Li, Q. Zhang, The vasorelaxant effect and its mechanisms of sodium bisulfite as a sulfur dioxide donor, Chemosphere 89 (2012) 579–584.
[11] Z. Meng, Vasodilator effect of gaseous sulfur dioxide and regulation of its level by Ach in rat vascular tissues, Inhal. Toxicol. 21 (2009) 1223–1228.
[12] M. Lovati, M. Daldossi, S. Sirtori, Effects of sub-chronic exposure to SO_2 on lipid and carbohydrate metabolism in rats, Arch. Toxicol. 70 (1996) 164–173.
[13] V.S. Lin, W. Chen, M. Xian, C.J. Chang, Chemical probes for molecular imaging and detection of hydrogen sulfide and reactive sulfur species in biological systems, Chem. Soc. Rev. 44 (2015) 4596–4618.
[14] G.J. Mohr, A chromoreactand for the selective detection of HSO_3^-based on the reversible bisulfite addition reaction in polymer membranes, Chem. Commun. 22 (2002) 2646–2647.
[15] Y. Li, M. Zhao, Simple methods for rapid determination of sulfite in food products, Food Control 17 (2006) 975–980.
[16] U.T. Yilmaz, G. Somer, Determination of trace sulfite by direct and indirect methods using differential pulse polarography, Anal. Chim. Acta 603 (2007) 30–35.
[17] D. Huang, B. Xu, J. Tang, J. Luo, L. Chen, L. Yang, Z. Yang, S. Bi, Indirect determination of sulfide ions in water samples at trace level by anodic stripping voltammetry using mercury film electrode, Anal. Methods 2 (2010) 154–158.
[18] S. Fäldt, B. Karlberg, W. Frenzel, Hyphenation of gas-diffusion separation and ion chromatography, Fresenius J. Anal. Chem. 371 (2001) 425–430.
[19] S. Theisen, R. Hansch, L. Kothe, U. Leist, R. Galensa, A fast and sensitive HPLC method for sulfite analysis in food based on a plant sulfite oxidase biosensor, Biosens. Bioelectron. 26 (2010) 175–181.
[20] Y. Huang, C. Zhang, X. Zhang, Z. Zhang, Chemiluminescence of sulfite based on auto-oxidation sensitized by rhodamine 6G, Anal. Chim. Acta 391 (1999) 95–100.
[21] D. Paulls, A. Townshen, Sensitized determination of sulfite using flow injection with chemiluminescent detection, Analyst 120 (1995) 467–469.
[22] B. Palenzuela, B.M. Simonet, A. Ríos, M. Valcárcel, Determination of free and total sulphur dioxide in wine by use of an amalgamated piezoelectric sensor, Anal. Chim. Acta 535 (2005) 65–72.
[23] V. Smith, Determination of sulfite using a sulfite oxidase enzyme electrode, Anal. Chem. 9 (1987) 2256–2259.
[24] S. Xu, R. Tang, Z. Wang, Y. Zhou, R. Yan, A novel flavone-based fluorescent probe for relay recognition of HSO_3^- and Al^{3+}, Spectrochim. Acta A Mol. Biomol. Spectrosc. 149 (2015) 208–215.
[25] X. Cheng, H. Jia, J. Feng, J. Qin, Z. Li, Reactive probe for hydrogen sulfite: turn-on fluorescent sensing and bioimaging application, J. Mater. Chem. B 1 (2013) 4110–4114.
[26] X.F. Yang, M. Zhao, G. Wang, A rhodamine-based fluorescent probe selective for bisulfite anion in aqueous ethanol media, Sens. Actuators B 152 (2011) 8–13.
[27] Y. Sun, C. Zhong, R. Gong, H. Mu, E. Fu, A ratiometric fluorescent chemodosimeter with selective recognition for sulfite in aqueous solution, J. Org. Chem. 74 (2009) 7943–7946.
[28] C. Wang, S. Feng, L. Wu, S. Yan, C. Zhong, P. Guo, R. Huang, X. Weng, X. Zhou, A new fluorescent turn-on probe for highly sensitive and selective detection of sulfite and bisulfite, Sens. Actuators B 190 (2014) 792–799.
[29] S. Chen, P. Hou, J. Wang, X. Song, A highly sulfite-selective ratiometric fluorescent probe based on ESIPT, RSC Adv. 2 (2012) 10869–10873.
[30] S.Y. Qu, H. Tian, Diketopyrrolopyrrole (DPP)-based materials for organic photovoltaics, Chem. Commun. 48 (2012) 3039–3051.
[31] J.W. Jung, F. Liu, T.P. Russell, W.H. Jo, A high mobility conjugated polymer based on dithienothiophene and diketopyrrolopyrrole for organic photovoltaics, Energy Environ. Sci. 5 (2012) 6857–6861.
[32] Q. Wang, J.J. Franeker, B.J. Bruijnaers, M.M. Wienk, R.A.J. Janssen, Structure-property relationships for bis-diketopyrrolopyrrole molecules in organic photovoltaics, J. Mater. Chem. A 4 (2016) 10532–10541.
[33] J.Y. Back, H. Yu, I. Song, I. Kang, H. Ahn, T.J. Shin, S.K. Kwon, J.H. Oh, Y.H. Kim, Investigation of structure-property relationships in diketopyrrolopyrrole-based polymer semiconductors via side-chain engineering, Chem. Mater. 27 (2015) 1732–1739.
[34] J.J. Yao, C.M. Yu, Z.T. Liu, H.W. Luo, Y. Yang, G.X. Zhang, D.Q. Zhang, Significant improvement of semiconducting performance of the diketopyrrolopyrrole-quaterthiophene conjugated polymer through side-chain engineering via hydrogen-bonding, J. Am. Chem. Soc. 138 (2016) 173–185.
[35] H. Yu, H.N. Kim, I. Song, Y.H. Ha, H. Ahn, J.H. Oh, Y.H. Kim, Effect of alkyl chain spacer on charge transport in n-type dominant polymer semiconductors with a diketopyrrolopyrrole-thiophene-bithiazole acceptor-donor-acceptor unit, J. Mater. Chem. C 5 (2017) 3616–3622.
[36] Y.T. Gao, G. Feng, T. Jiang, C. Goh, L. Ng, B. Liu, B. Li, L. Yang, J. Hua, H. Tian, Biocompatible nanoparticles based on diketo-pyrrolo-pyrrole (DPP) with aggregation-induced red/NIR emission for in Vivo two-photon fluorescence imaging, Adv. Funct. Mater. 25 (2015) 2857–2866.
[37] H. Ftouni, F. Bolze, H. Rocquigny, J.F. Nicoud, Functionalized two-photon absorbing diketopyrrolopyrrole-based fluorophores for living cells fluorescent microscopy, Bioconjugate Chem. 24 (2013) 942–950.
[38] Y. Qu, J.L. Hua, H. Tian, Colorimetric and ratiometric red fluorescent chemosensor for fluoride ion based on diketopyrrolopyrrole, Org. Lett. 12 (2010) 3320–3323.
[39] W.S. Qu, L. Yang, Y.D. Hang, X. Zhang, Y. Qu, J.L. Hua, Photostable red turn-on fluorescent diketopyrrolopyrrole chemodosimeters for the detection of cysteine in living cells, Sens. Actuators B 211 (2015) 275–282.
[40] X. Zhang, Y.D. Hang, W.S. Qu, Y.Y. Yan, P. Zhao, J.L. Hua, Diketopyrrolopyrrole-based ratiometric fluorescent probe for the sensitive and selective detection of cysteine over homocysteine and glutathione in living cells, RSC Adv. 6 (2016) 20014–20020.
[41] D. Aigner, B. Ungerbock, T. Mayr, R. Saf, I. Klimanta, S.M. Borisov, Fluorescent materials for pH sensing and imaging based on novel 1,4-diketopyrrolo-[3,4-c] pyrrole dyes, J. Mater. Chem. C 1 (2013) 5685–5693.
[42] M. Kaur, M.J. Cho, D.H. Choi, Chemodosimeter approach: selective detection of fluoride ion using a diketopyrrolopyrrole derivative, Dyes Pigm. 103 (2014) 154–160.
[43] L.Y. Wang, J.Q. Du, D.R. Cao, A colorimetric fluorescent chemodosimeter based on diketopyrrolopyrrole and 1,3-indanedione for cysteine detection and cellular imaging in living cells, Sens. Actuators B 205 (2014) 281–288.
[44] H. Burckstummer, A. Weissenstein, D. Bialas, F. Wurthner, Synthesis and characterization of optical and redox properties of bithiophene-functionalized diketopyrrolopyrrole chromophores, J. Org. Chem. 76 (2011) 2426–2432.
[45] T. Yamagata, J. Kuwabara, T. Kanbara, Synthesis of highly fluorescent diketopyrrolopyrrole derivative and two-step response of fluorescence to acid, Tetrahedron Lett. 51 (2010) 1596–1599.
[46] M. Grzybowski, E.G. Mrowka, V. Hugues, W. Brutkowski, M.B. Desce, D.T. Gryko, Polar diketopyrrolopyrrole-imidazolium salts as selective probes for staining mitochondria in two-photon fluorescence microscopy, Chem. Eur. J. 21 (2015) 9101–9110.
[47] X. Yang, Y. Cui, Y. Li, L. Zheng, L. Xie, R. Ning, Z. Liu, J. Lu, G. Zhang, C. Liu, G. Zhang, A new diketopyrrolopyrrole-based probe for sensitive and selective detection of sulfite in aqueous solution, Spectrochim. Acta A Mol Biomol. Spectrosc. 137 (2015) 1055–1060.
[48] D.Y. Lee, M.K. Jung, J. Yin, G. Kim, C.G. Pack, J.Y. Yoon, An aniline bearing hemicyanine derivative serves as a mitochondria selective probe, Dyes Pigm. 136 (2017) 467–472.
[49] S.Y. Lim, K.H. Hong, D. Kim, H.K. Kwon, H.J. Kim, Tunable heptamethine-azo dye conjugate as an NIR fluorescent probe for the selective detection of mitochondrial glutathione over cysteine and homocysteine, J. Am. Chem. Soc. 136 (2014) 7018–7025.
[50] E. Wang, L. Pang, Y. Zhou, J. Zhang, F. Yu, H. Qiao, X. Pang, A high performance Schiff-base fluorescent probe for monitoring Au^{3+} in zebrafish based on BODIPY, Biosens. Bioelectron. 77 (2016) 812–817.
[51] M. Morton, H. Landfie, Kinetics of bisulfite addition to α, β-unsaturated compound, Maurice Mortor Harold Landfield 74 (1952) 3523–3526.
[52] D. Li, Y. Shi, X. Tian, M. Wang, B. Huang, F. Li, S. Li, H. Zhou, J. Wu, Y. Tian, Fluorescent probes with dual-mode for rapid detection of SO_2 derivatives in living cells: ratiometric and two-photon fluorescent sensors, Sens. Actuators B 233 (2016) 1–6.
[53] H.D. Li, Q.C. Yao, J.L. Fan, C. Hu, F. Xu, J.J. Du, J.Y. Wang, X.J. Peng, A fluorescent probe for ratiometric imaging of SO_2 derivatives in mitochondria of living cells, Ind. Eng. Chem. Res. 55 (2016) 1477–1483.
[54] Y.Q. Sun, J. Liu, J.Y. Zhang, T. Yang, W. Guo, Fluorescent probe for biological gas SO_2 derivatives bisulfite and sulfite, Chem. Commun. 49 (2013) 2637–2639.
[55] Y. Liu, K. Li, K.X. Xie, L.L. Li, K.K. Yu, X. Wang, X.Q. Yu, A water-soluble and fast-response mitochondria-targeted fluorescent probe for colorimetric and ratiometric sensing of endogenously generated SO_2 derivatives in living cells, Chem. Commun. 52 (2016) 3430–3433.